

Cooperative Training of Fast Thinking Initializer and Slow Thinking Solver for Multi-Modal Conditional Learning

Jianwen Xie*, Zilong Zheng*, Xiaolin Fang, Song-Chun Zhu, *Fellow, IEEE*, and Ying Nian Wu

Abstract—This paper studies the supervised learning of the conditional distribution of a high-dimensional output given an input, where the output and input may belong to two different modalities, e.g., the output is an photo image and the input is a sketch image. We solve this problem by cooperative training of a fast thinking initializer and slow thinking solver. The initializer generates the output directly by a non-linear transformation of the input as well as a noise vector that accounts for latent variability in the output. The slow thinking solver learns an objective function in the form of a conditional energy function, so that the output can be generated by optimizing the objective function, or more rigorously by sampling from the conditional energy-based model. We propose to learn the two models jointly, where the fast thinking initializer serves to initialize the sampling of the slow thinking solver, and the solver refines the initial output by an iterative algorithm. The solver learns from the difference between the refined output and the observed output, while the initializer learns from how the solver refines its initial output. We demonstrate the effectiveness of the proposed method on various multi-modal conditional learning tasks, e.g., class-to-image generation, image-to-image translation, and image recovery.

Index Terms—Deep generative models; Generative cooperative learning; Multi-modal conditional learning.

1 INTRODUCTION

1.1 Background and motivation

WHEN we learn to solve a problem, we can learn to directly map the problem to the solution. This amounts to fast thinking, which underlies reflexive or impulsive behavior, or muscle memory, and it can happen when one is emotional or under time constraint. We may also learn an objective function or value function that assigns values to candidate solutions, and we optimize the objective function by an iterative algorithm to find the most valuable solution. This amounts to slow thinking, which underlies planning, searching or optimal control, and it can happen when one is calm or have time to think through.

In this paper, we study the supervised learning of the conditional distribution of a high-dimensional output given an input, where the output and input may belong to two different modalities. For instance, the output may be an image, while the input may be a class label, a sketch, or an image from another domain. The input defines the problem, and the output is the solution. We also refer to the input as the source or condition, and the output as the target.

We solve this problem by learning two models cooperatively. One model is an initializer. It generates the output directly by a non-linear transformation of the input as well as a noise vector, where the noise vector is to account for variability or uncertainty in

the output. This amounts to fast thinking because the conditional generation is accomplished by direct mapping. The other model is a solver. It learns an objective function in the form of a conditional energy function, so that the output can be generated by optimizing the objective function, or more rigorously by sampling from the conditional energy-based model, where the sampling is to account for variability and uncertainty. This amounts to slow thinking because the sampling is accomplished by an iterative algorithm such as Langevin dynamics, which is an example of Markov chain Monte Carlo (MCMC). We propose to learn the two models jointly, where the initializer serves to initialize the sampling of the solver, and the solver refines the initial solution by an iterative algorithm. The solver learns from the difference between the refined solution and the observed solution, while the initializer learns from the difference between the initial solution and the refined solution.

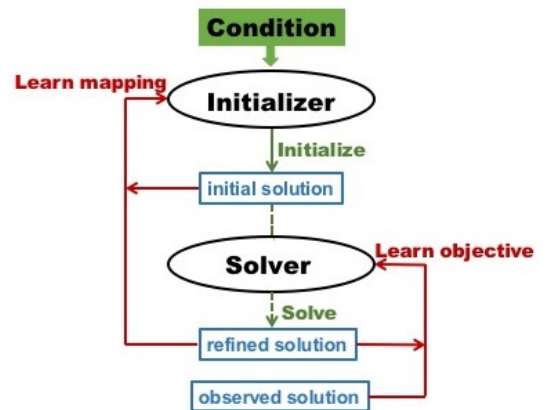
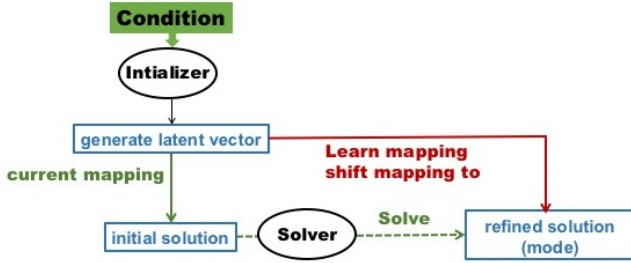


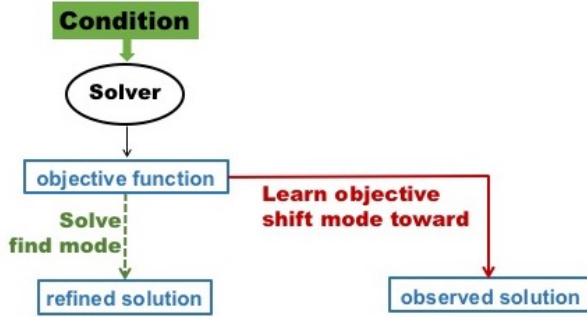
Fig. 1. The initializer initializes the solver, which refines the initial solution. The initializer learns from the solver's refinement, while the solver learns by comparing to the observed solution.

- J. Xie is with Hikvision Research Institute, Santa Clara, USA. E-mail: jianwen@ucla.edu
- Z. Zheng is with the Department of Computer Science, University of California, Los Angeles, USA. E-mail: zilongzheng0318@ucla.edu
- X. Fang is with the Department of Computer Science, Massachusetts Institute of Technology, USA. E-mail: xiaolinf@csail.mit.edu
- S.-C. Zhu is with the Department of Statistics, University of California, Los Angeles, USA. E-mail: sczhu@stat.ucla.edu
- Y. N. Wu is with the Department of Statistics, University of California, Los Angeles, USA. E-mail: ywu@stat.ucla.edu
- * indicates equal contributions.

Figure 1 conveys the basic idea. The algorithm iterates two steps, a solving step and a learning step. The solving step consists of two stages: **Initialize**: The initializer generates the initial solution. **Solve**: The solver refines the initial solution. The learning step also consists of two parts: **Learn-mapping**: The initializer learns from how the solver refines its initial solution. **Learn-objective**: The solver updates its objective function by shifting its high value region from the refined solution to the observed solution.



(a) Learn-mapping by mapping shift.



(b) Learn-objective by objective shift.

Fig. 2. (a) **Learn-mapping by mapping shift**: the initializer shifts its mapping toward the refined solution. (b) **Learn-objective by objective shift**: the solver shifts the high value region or mode of its objective function toward the observed solution.

Figure 2(a) illustrates Learn-mapping step. In the Initialization step, the initializer generates the latent noise vector, which, together with the input condition, is mapped to the initial solution. In the Learn-mapping step, the initializer updates its parameters so that it maps the input condition and the latent vector to the refined solution, in order to absorb the refinement made by the solver. Because the latent vector is known, it does not need to be inferred and the learning is easy.

Figure 2(b) illustrates Learn-objective step. In the Solve step, the solver finds the refined solution at high value region around a mode of the objective function. In the Learn-objective step, the solver updates its parameters so that the objective function shifts its high value region around the mode toward the observed solution, so that in the next iteration, the refined solution will get closer to the observed solution.

The solver shifts its mode toward the observed solution, while inducing the initializer maps the input condition and the latent vector to its mode. Learning an initializer is like mimicking “how”, while learning a solver is like trying to understand “why” in terms of goal or value underlying the action.

Why slow thinking solver? The reason we need a solver in addition to an initializer is that it is often easier to learn the objective function than learning to generate the solution directly, since it is always easier to demand or desire something than to actually produce something directly. Because of its relative simplicity, the

learned objective function can be more generalizable than the learned initializer. For instance, in an unfamiliar situation, we tend to be tentative, relying on slow thinking planning rather than fast thinking habit.

Efficiency. Even though we use the wording “slow thinking”, it is only relative to “fast thinking”. In fact, the slow thinking solver is usually fast enough, especially if it is jumpstarted by fast thinking initializer, and there is no problem scaling up our method to big datasets. Therefore the time efficiency of the slow thinking method is not a concern.

Student-teacher v.s. actor-critic. We may consider the initializer as a student model, and the solver as a teacher model. The teacher refines the initial solution of the student by a refinement process, and distills the refinement process into the student. This is different from the actor-critic relationship in (inverse) reinforcement learning [1], [2], [3] because the critic does not refine the actor’s solution by a slow thinking process.

Associative memory. The two models may also be considered as associative memory [4]. While the initializer is like sudden recall, the solver is like rumination, filling in and playing out details.

Cooperative learning v.s. adversarial learning. Our framework, belonging to cooperative learning, jointly learns a conditional energy-based model and a conditional generator. This is different from conditional generative adversarial nets (CGANs), where a conditional discriminator is simultaneously learned to help train the conditional generator. Unlike CGANs, our framework enables refinement by Langevin sampling. Additionally, our framework simultaneously trains both sub models and keep both of them after training, but CGANs will discard the discriminator once the generator mode is well trained.

We apply our learning method to various conditional image generation tasks. Our experiments show that the proposed method is effective compared to other methods, such as those based on GANs [5].

Contributions. This paper proposes a novel method for supervised learning of high-dimensional conditional distributions by learning a fast thinking initializer and a slow thinking solver. We show the effectiveness of our method on conditional image generation and recovery tasks. Perhaps more importantly, (1) we propose a different method for conditional learning than GAN-based methods. Unlike GAN methods, our method has a learned value function to guide a slow thinking process to further refine the solution of the initializer (i.e., conditional generator), and our work has demonstrated the benefit of such a refinement on various image generation tasks. (2) The proposed strategy may be applied to a broad range of AI problems that can be modeled via a conditional learning framework, e.g., inverse optimal control, etc. The interaction between the fast thinking initializer and the slow thinking solver can be of interest to cognitive science. (3) This is the first paper to study conditional learning via a model-based Initializer-solver framework. It is fundamental and important to AI community.

1.2 Related work

The following are related themes of research.

Conditional adversarial learning. A popular method of multimodal learning is conditional GANs. For example, [6], [7] use conditional GAN for image synthesis based on class labels. [8], [9] study text-conditioned image synthesis. Other examples include multimodal image-to-image mapping [10], image-to-image

translation [11], [12], [13], and super-resolution [14]. Our work studies similar problems. The difference is that our method is based on a conditional energy function and an iterative algorithm guided by this objective function. Existing adversarial learning methods, including those in inverse reinforcement learning [3], do not involve this slow thinking solving process.

Cooperative learning. Just as the conditional GAN is inspired by the original GAN [5], our learning method is inspired by the recent work of [15], where the models are unconditioned. While unconditioned generation is interesting, conditional generation and recovery is much more useful in applications. It is also much more challenging because we need to incorporate the input condition into both the initializer and the solver. Thus our method is a substantial generalization of [15], and our extensive experiments convincingly demonstrate the usefulness of our method, which in the mean time provides a different methodology from GAN-based methods.

Conditional random field. The objective function and the conditional energy-based model can also be considered a form of conditional random field [16]. Unlike traditional conditional random field, our conditional energy function is defined by a deep network, and its sampling process is jumpstarted by an initializer.

Multimodal generative learning. Learning joint probability distribution of signals of different modalities enables us to recover or generate one modality based on other modalities. For example, [17] learns a dual-wing harmoniums model for image and text data. [18] learns stacked multimodal auto-encoder on video and audio data. [19] learns a multimodal deep Boltzmann machine for joint image and text modeling. Our work focuses on the conditional distribution of one modality given another modality, and our method involves the cooperation between two types of models.

Energy-based generative neural nets. Our slow thinking solver is related to energy-based generative neural nets [20], [21], [22], [23], [24], [25], [26], which are energy-based models (EBMs) with energy functions parameterized by deep neural nets, and trained by MCMC-based maximum likelihood learning. [20] is the first to learn EBMs parametrized by modern ConvNets by maximum likelihood estimation via Langevin dynamics, and also investigates ReLU [27] with Gaussian reference in the proposed model that are called generative ConvNet. [21] proposes a multi-grid sampling and learning method for the generative ConvNet. [22], [23] generalize [20] for modeling dynamic patterns by adopting a spatial-temporal ConvNet in the energy function. [24] develops a volumetric version of the energy-based generative neural net for 3D object patterns. Recently, [25] investigates training the energy-based generative ConvNets with short-run MCMC. All models mentioned above are unconditioned EBMs, while our solver is a conditioned EBM jointly trained with a conditional generator serving as an approximate sampler.

Inverse reinforcement learning. Our method is related to inverse reinforcement learning and inverse optimal control [1], [2], where the initializer corresponds to the policy, and the solver corresponds to the planning or optimal control. Unlike the action space in reinforcement learning, the output in our work is of a much higher dimension, a fact that also distinguishes our work from common supervised learning problem such as classification. As a result, the initializer needs to transform a latent noise vector to generate the initial solution, and this is different from the policy in reinforcement learning, where the policy is defined by the conditional distribution of action given state, without resorting to a latent vector.

2 COOPERATIVE CONDITIONAL LEARNING

Let Y be the D -dimensional output signal of the target modality, and C be the input signal of the source modality, where “C” stands for “condition”. C defines the problem, and Y is the solution. Our goal is to learn the conditional distribution $p(Y|C)$ of the target signal (solution) Y given the source signal C (problem) as the condition. We shall learn $p(Y|C)$ from the training dataset of the pairs $\{(Y_i, C_i), i = 1, \dots, n\}$ with the fast thinking initializer and slow thinking solver.

2.1 Slow thinking solver

The solver is based an objective function or value function $f(Y, C; \theta)$ defined on (Y, C) . $f(Y, C; \theta)$ can be parametrized by a bottom-up convolutional network (ConvNet) where θ collects all the weight and bias parameters. Serving as a negative energy function, $f(Y, C; \theta)$ defines a joint energy-based model [20]:

$$p(Y, C; \theta) = \frac{1}{Z(\theta)} \exp [f(Y, C; \theta)], \quad (1)$$

where $Z(\theta) = \int \exp [f(Y, C; \theta)] dY dC$ is the normalizing constant.

Fixing the source signal C , $f(Y, C; \theta)$ defines the value of the solution Y for the problem defined by C , and $-f(Y, C; \theta)$ defines the conditional energy function. The conditional probability is given by

$$\begin{aligned} p(Y|C; \theta) &= \frac{p(Y, C; \theta)}{p(C; \theta)} = \frac{p(Y, C; \theta)}{\int p(Y, C; \theta) dY} \\ &= \frac{1}{Z(C, \theta)} \exp [f(Y, C; \theta)], \end{aligned} \quad (2)$$

where $Z(C, \theta) = Z(\theta)p(C; \theta)$. The learning of this model seeks to maximize the conditional log-likelihood function

$$L(\theta) = \frac{1}{n} \sum_{i=1}^n \log p(Y_i|C_i; \theta), \quad (3)$$

whose gradient $L'(\theta)$ is

$$\sum_{i=1}^n \left\{ \frac{\partial}{\partial \theta} f(Y_i, C_i; \theta) - E_{p(Y|C_i, \theta)} \left[\frac{\partial}{\partial \theta} f(Y, C_i; \theta) \right] \right\}, \quad (4)$$

where $E_{p(Y|C; \theta)}$ denotes the expectation with respect to $p(Y|C, \theta)$. The identity underlying (4) is $\frac{\partial}{\partial \theta} \log Z(C, \theta) = E_{p(Y|C, \theta)} \left[\frac{\partial}{\partial \theta} f(Y, C; \theta) \right]$.

The expectation in (4) is analytically intractable and can be approximated by drawing samples from $p(Y|C, \theta)$ and then computing the Monte Carlo average. This can be solved by an iterative algorithm, which is a slow thinking process. One solver is the Langevin dynamics for sampling $Y \sim p(Y|C, \theta)$. It iterates the following step:

$$Y_{\tau+1} = Y_{\tau} + \frac{\delta^2}{2} \frac{\partial}{\partial Y} f(Y_{\tau}, C; \theta) + \delta U_{\tau}, \quad (5)$$

where τ indexes the time steps of the Langevin dynamics, δ is the step size, and $U_{\tau} \sim N(0, I_D)$ is Gaussian white noise. D is the dimensionality of Y . A Metropolis-Hastings acceptance-rejection step can be added to correct for finite δ . The Langevin dynamics is gradient descent on the energy function, plus noise for diffusion so that it samples the distribution instead of being trapped in the local modes.

For each observed condition C_i , we run the Langevin dynamics according to (5) to obtain the corresponding synthesized example \tilde{Y}_i as a sample from $p(Y|C_i, \theta)$. The Monte Carlo approximation to $L'(\theta)$ is

$$L'(\theta) \approx \frac{\partial}{\partial \theta} \left[\frac{1}{n} \sum_{i=1}^n f(Y_i, C_i; \theta) - \frac{1}{n} \sum_{i=1}^n f(\tilde{Y}_i, C_i; \theta) \right]. \quad (6)$$

We can then update $\theta^{(t+1)} = \theta^{(t)} + \gamma_t L'(\theta^{(t)})$.

Objective shift: The above gradient ascent algorithm is to increase the average value of the observed solutions versus that of the refined solutions, i.e., on average, it shifts high value region or mode of $f(Y, C_i; \theta)$ from the generated solution \tilde{Y}_i toward the observed solution Y_i .

The convergence of such a stochastic gradient ascent algorithm has been studied by [28].

2.2 Fast thinking initializer

The initializer is of the following form:

$$X \sim N(0, I_d), Y = g(X, C; \alpha) + \epsilon, \epsilon \sim N(0, \sigma^2 I_D), \quad (7)$$

where X is the d -dimensional latent noise vector, and $g(X, C; \alpha)$ is a top-down ConvNet defined by the parameters α . The ConvNet g maps the observed condition C and the latent noise vector X to the signal Y directly. If the source signal C is of high dimensionality, we can parametrize g by an encoder-decoder structure: we first encode C into a latent vector Z , and then we map (X, Z) to Y by a decoder. Given C , we can generate Y from the conditional generator model by direct sampling, i.e., first sampling X from its prior distribution, and then mapping (X, Z) into Y directly. This is fast thinking without iteration.

We can learn the initializer from the training pairs $\{(Y_i, C_i), i = 1, \dots, n\}$ by maximizing the conditional log-likelihood $L(\alpha) = \frac{1}{n} \sum_{i=1}^n \log p(Y_i|C_i, \alpha)$, where $p(Y|C, \alpha) = \int p(X)p(Y|C, X, \alpha)dX$. The learning algorithm iterates the following two steps. (1) Sample X_i from $p(X_i|Y_i, C_i, \alpha)$ by Langevin dynamics. (2) Update α by gradient descent on $\frac{1}{n} \sum_{i=1}^n \|Y_i - g(X_i, C_i; \alpha)\|^2$. See [29] for details.

2.3 Cooperative training of initializer and solver

The initializer and the solver can be trained jointly as follows.

(1) The initializer supplies initial samples for the MCMC of the solver. For each observed condition input C_i , we first generate $\hat{X}_i \sim N(0, I_d)$, and then generate the initial solution $\hat{Y}_i = g(\hat{X}_i, C_i; \alpha) + \epsilon_i$. If the current initializer is close to the current solver, then the generated $\{\hat{Y}_i, i = 1, \dots, n\}$ should be a good initialization for the solver to sample from $p(Y|C_i, \theta)$, i.e., starting from the initial solutions $\{\hat{Y}_i, i = 1, \dots, n\}$, we run Langevin dynamics for l steps to get the refined solutions $\{\tilde{Y}_i, i = 1, \dots, n\}$. These $\{\tilde{Y}_i\}$ serve as the synthesized examples from $p(Y|C_i)$ and are used to update θ in the same way as we learn the solver model in equation (6) for objective shifting.

(2) The initializer then learns from the MCMC. Specifically, the initializer treats $\{(\tilde{Y}_i, C_i), i = 1, \dots, n\}$ produced by the MCMC as the training data. The key is that these $\{\tilde{Y}_i\}$ are obtained by the Langevin dynamics initialized from the $\{\hat{Y}_i, i = 1, \dots, n\}$, which are generated by the initializer with *known* latent noise vectors $\{\hat{X}_i, i = 1, \dots, n\}$. Given $\{(\hat{X}_i, \tilde{Y}_i, C_i), i = 1, \dots, n\}$, we can learn α by minimizing $\frac{1}{n} \sum_{i=1}^n \|\tilde{Y}_i - g(\hat{X}_i, C_i; \alpha)\|^2$, which is a

nonlinear regression of \tilde{Y}_i on (\hat{X}_i, C_i) . This can be accomplished by gradient descent

$$\Delta \alpha \propto -(\tilde{Y}_i - g(\hat{X}_i, C_i; \alpha)) \frac{\partial}{\partial \alpha} g(\hat{X}_i, C_i; \alpha). \quad (8)$$

Mapping shift: Initially $g(X, C; \alpha)$ maps (\hat{X}_i, C_i) to the initial solution \hat{Y}_i . After updating α , $g(X, C; \alpha)$ maps (\hat{X}_i, C_i) to the refined solution \tilde{Y}_i . Thus the updating of α absorbs the MCMC transitions that change \hat{Y}_i to \tilde{Y}_i . In other words, we distill the MCMC transitions of the refinement process into $g(X, C; \alpha)$.

Algorithm 1 presents a description of the conditional learning with two models. See Figures 1 and 2 for illustrations.

Both computations can be carried out by back-propagation, and the whole algorithm is in the form of alternating back-propagation.

Algorithm 1 Conditional Learning

Input:

- (1) training examples $\{(Y_i, C_i), i = 1, \dots, n\}$
- (2) numbers of Langevin steps l
- (3) number of learning iterations T .

Output:

- (1) learned parameters θ and α ,
- (2) generated examples $\{\hat{Y}_i, \tilde{Y}_i, i = 1, \dots, n\}$.

- 1: $t \leftarrow 0$, initialize θ and α .
 - 2: **repeat**
 - 3: **Initialization by mapping:** For $i = 1, \dots, n$, generate $\hat{X}_i \sim N(0, I_d)$, and generate the initial solution $\hat{Y}_i = g(\hat{X}_i, C_i; \alpha^{(t)}) + \epsilon_i$.
 - 4: **Solve based on objective:** For $i = 1, \dots, n$, starting from \hat{Y}_i , run l steps of Langevin dynamics to obtain the refined solution \tilde{Y}_i , each step following equation (5).
 - 5: **Learn-objective by objective shift:** Update $\theta^{(t+1)} = \theta^{(t)} + \gamma_t L'(\theta^{(t)})$, where $L'(\theta^{(t)})$ is computed according to (6).
 - 6: **Learn-mapping by mapping shift:** Update $\alpha^{(t+1)} = \alpha^{(t)} + \gamma_t \Delta \alpha^{(t)}$, where $\Delta \alpha^{(t)}$ is computed according to (8)
 - 7: Let $t \leftarrow t + 1$
 - 8: **until** $t = T$
-

In Algorithm 1, the conditional descriptor model is the primary model for conditional synthesis or recovery by MCMC sampling. The conditional generator model plays an assisting role to initialize the MCMC sampling.

Model convergence. The convergence is discussed in the supplementary materials as a theoretical understanding of our learning method. We summarize the key idea as follows. Let $M(Y_1|Y_0, C; \theta)$ be the transition kernel of the finite-step MCMC that refines the initial solution Y_0 to the refined solution Y_1 . Let $(M_\theta q)(Y_1|C; \alpha) = \int M(Y_1|Y_0, C; \theta)q(Y_0|C; \alpha)dY_0$ be the distribution obtained by running the finite-step MCMC from the initializer distribution $q(Y_0|C; \alpha)$.

In the limit, if the algorithm converges to a fixed point, then the resulting initializer $q(Y|C; \alpha)$ minimizes $KL((M_\theta q)(Y|C; \alpha) \| q(Y|C; \alpha))$, that is, $q(Y|C; \alpha)$ seeks to be the stationary distribution of the MCMC transition M_θ , which is the solver $p(Y|C; \theta)$.

If the learned $q(Y|C; \alpha)$ is close to $p(Y|C; \theta)$, then $(M_\theta q)(Y|C; \alpha)$ is even closer to $p(Y|C; \theta)$. Then the learned solver $p(Y|C; \theta)$ is close to MLE, i.e., minimizing $KL(P_{\text{data}}(Y|C) \| p(Y|C; \theta))$.

3 THEORETICAL UNDERPINNING

This section presents theoretical underpinnings of the model and the learning algorithms presented in the previous section. Readers who are more interested in applications and experiments can jump to the next section.

3.1 Kullback-Leibler divergence

The Kullback-Leibler divergence between two distributions $p(x)$ and $q(x)$ is defined as $\text{KL}(p||q) = \mathbb{E}_p[\log(p(X)/q(X))]$.

The Kullback-Leibler divergence between two conditional distributions $p(y|x)$ and $q(y|x)$ is defined as

$$\text{KL}(p||q) = \mathbb{E}_p \left[\log \frac{p(Y|X)}{q(Y|X)} \right] \quad (9)$$

$$= \int \log \frac{p(y|x)}{q(y|x)} p(x, y) dx dy, \quad (10)$$

where the expectation is over the joint distribution $p(x, y) = p(x)p(y|x)$.

3.2 Slow thinking solver

The slow thinking solver model is

$$\begin{aligned} p(Y|C; \theta) &= \frac{p(Y, C; \theta)}{p(C; \theta)} = \frac{p(Y, C; \theta)}{\int p(Y, C; \theta) dY} \\ &= \frac{1}{Z(C; \theta)} \exp[f(Y, C; \theta)], \end{aligned} \quad (11)$$

where

$$Z(C; \theta) = \int \exp[f(Y, C; \theta)] dY \quad (12)$$

is the normalizing constant and is analytically intractable.

Suppose the training examples $\{(Y_i, C_i), i = 1, \dots, n\}$ are generated by the true joint distribution $f(Y, C)$, whose conditional distribution is $f(Y|C)$.

For large sample $n \rightarrow \infty$, the maximum likelihood estimation of θ is to minimize the Kullback-Leibler divergence

$$\min_{\theta} \text{KL}(f(Y|C)||p(Y|C; \theta)). \quad (13)$$

In practice, the expectation with respect to $f(Y, C)$ is approximated by the sample average. The difficulty with $\text{KL}(f(Y|C)||p(Y|C; \theta))$ is that the $\log Z(C; \theta)$ term is analytically intractable, and its derivative has to be approximated by MCMC sampling from the model $p(Y|C; \theta)$.

3.3 Fast thinking initializer

The fast thinking initializer is

$$X \sim N(0, I_d), Y = g(X, C; \alpha) + \epsilon, \epsilon \sim N(0, \sigma^2 I_D). \quad (14)$$

We use the notation $q(Y|C; \alpha)$ to denote the resulting conditional distribution. It is obtained by

$$q(Y|C; \alpha) = \int q(X)q(Y|X, C; \alpha) dX, \quad (15)$$

which is analytically intractable.

For large sample, the maximum likelihood estimation of α is to minimize the Kullback-Leibler divergence

$$\min_{\alpha} \text{KL}(f(Y|C)||q(Y|C; \alpha)). \quad (16)$$

Again, the expectation with respect to $f(Y, C)$ is approximated by the sample average. The difficulty with $\text{KL}(f(Y|C)||q(Y|C; \alpha))$ is that $\log q(Y|C; \alpha)$ is analytically intractable, and its derivative has to be approximated by MCMC sampling of the posterior $q(X|Y, C; \alpha)$.

3.4 Objective shift: modified contrastive divergence

Let $M(Y_1|Y_0, C; \theta)$ be the transition kernel of the finite-step MCMC that refines the initial solution Y_0 to the refined solution Y_1 . Let $(M_{\theta}q)(Y_1|C; \alpha) = \int M(Y_1|Y_0, C; \theta)q(Y_0|C; \alpha)dY_0$ be the distribution obtained by running the finite-step MCMC from $q(Y_0|C; \alpha)$.

Given the current initializer $q(Y|C; \alpha)$, the objective shift updates θ_t to θ_{t+1} , and the update approximately follows the gradient of the following modified contrastive divergence [15], [30]

$$\begin{aligned} &\text{KL}(f(Y|C)||p(Y|C; \theta)) \\ &- \text{KL}((M_{\theta_t}q)(Y|C; \alpha)||p(Y|C; \theta)). \end{aligned} \quad (17)$$

Compare (17) with the MLE (11), (17) has the second divergence term $\text{KL}((M_{\theta_t}q)(Y|C; \alpha)||p(Y|C; \theta))$ to cancel the $\log Z(C; \theta)$ term, so that its derivative is analytically tractable. The learning is to shift $p(Y|C; \theta)$ or its high value region around the mode from the refined solution provided by $(M_{\theta_t}q)(Y|C; \alpha)$ toward the observed solution given by $f(Y|C)$. If $(M_{\theta_t}q)(Y|C; \alpha)$ is close to $p(Y|C; \theta)$, then the second divergence is close to zero, and the learning is close to MLE update.

3.5 Mapping shift: distilling MCMC

Given the current solver model $p(Y|C; \theta)$, the mapping shift updates α_t to α_{t+1} , and the update approximately follows the gradient of

$$\text{KL}((M_{\theta}q)(Y|C; \alpha_t)||q(Y|C; \alpha)). \quad (18)$$

This update distills the MCMC transition M_{θ} into the model $q(Y|C; \alpha)$. In the idealized case where the above divergence can be minimized to zero, then $q(Y|C; \alpha_{t+1}) = (M_{\theta}q)(Y|C; \alpha_t)$. The limiting distribution of the MCMC transition M_{θ} is $p(Y|C; \theta)$, thus the cumulative effect of the above update is to lead $q(Y|C; \alpha)$ close to $p(Y|C; \theta)$.

Compare (18) to the MLE (14), the training data distribution becomes $(M_{\theta}q)(Y|C; \alpha_t)$ instead of $f(Y|C)$. That is, $q(Y|C; \alpha)$ learns from how M_{θ} refines it. The learning is accomplished by mapping shift where the generated latent vector X is known, thus does not need to be inferred (or the Langevin inference algorithm can initialize from the generated X). In contrast, if we are to learn from $f(Y|C)$, we need to infer the unknown X by sampling from the posterior distribution.

In the limit, if the algorithm converges to a fixed point, then the resulting $q(Y|C; \alpha)$ minimizes $\text{KL}((M_{\theta}q)(Y|C; \alpha)||q(Y|C; \alpha))$, that is, $q(Y|C; \alpha)$ seeks to be the stationary distribution of the MCMC transition M_{θ} , which is $p(Y|C; \theta)$.

If the learned $q(Y|C; \alpha)$ is close to $p(Y|C; \theta)$, then $(M_{\theta_t}q)(Y|C; \alpha)$ is even closer to $p(Y|C; \theta)$. Then the learned $p(Y|C; \theta)$ is close to MLE because the second divergence term in (17) is close to zero.

4 EXPERIMENTS

We test the proposed framework for multimodal conditional learning on a variety of tasks. According to the form of the conditional learning, we organize the experiments into two parts. In the first part (Experiment 1), we study conditional learning for a mapping from category (one-hot vector) to image, e.g., image generation conditioned on class, while in the second part (Experiment 2), we study conditional learning for a mapping from image to image, e.g., image-to-image translation. We propose a specific network architecture of our model in each experiment due to the different forms of input-output modality. Unlike the unconditioned cooperative learning framework [31], the conditioned framework needs to find a proper way to fuse the condition C into both the bottom-up ConvNet f in the solver and the top-down ConvNet g in the initializer, for the sake of capturing accurate conditioning information. An improper design can cause not only unrealistic but also condition-mismatched synthesized results.

4.1 Experiment 1: Category \rightarrow Image

4.1.1 Network architecture

We start from learning the conditional distribution of an image given a category or class label. The category information is encoded as a one-hot vector. The network architecture of the model in this experiment is given as follows.

In the initializer, we can concatenate the one-hot vector C_i with the latent noise vector X sampled from $N(0, I_d)$ as the input of the top-down ConvNet to build a conditional generator $g(X, C; \alpha)$. The generator maps the input into image Y by several layers of deconvolutions. We call this setting “early concatenation”. (See Figure 3(1) for an illustration.) We can also adopt an architecture with “late concatenation”, where the concatenation happens in the intermediate layer of the initializer. Specifically, we can first sample the latent noise vector X from Gaussian noise prior $N(0, I_d)$, and then decode X to an intermediate result with spatial dimension $b \times b$ by a decoder $\Psi(X; \psi)$, which is parameterized by ψ and consists of several layers of deconvolutions with batch normalization [32] followed by ReLU non-linear transformation. We then replicate the one-hot vector C spatially and perform a channel concatenation with the intermediate output. After that, we generate the target image from the concatenated result by a generator $g(\Psi(X; \psi), C; \alpha)$ that performs several layers of deconvolutions. Batch normalization and ReLU layers are used between deconvolution layers and tanh non-linearity is added at the bottom layer. (See Figure 3(2) for an illustration.) The details of the networks will be mentioned in the section of each experiment.

To build the negative energy function for the solver model, in the setting of “early concatenation”, we first replicate the condition one-hot vector C spatially and perform a depth concatenation with image Y , and then map them to the negative energy by a bottom-up ConvNet, $f(Y, C; \theta)$, that consists of several layers of convolutions and ReLU non-linear transformation. (See Figure 4(1) for an illustration.) As to the “late concatenation”, we first encode the image Y to an intermediate result with spatial dimension $a \times a$ by an encoder $\Phi(Y; \phi)$, which is parameterized by ϕ and consists of several layers of convolutions followed by ReLU non-linear transformation, and then we replicate the one-hot vector C spatially and perform a depth concatenation with the intermediate result. The negative energy function is defined by a bottom-up ConvNet $f(\Phi(Y; \phi), C; \theta)$, which takes as input the concatenated result and outputs the negative energy by performing several layers

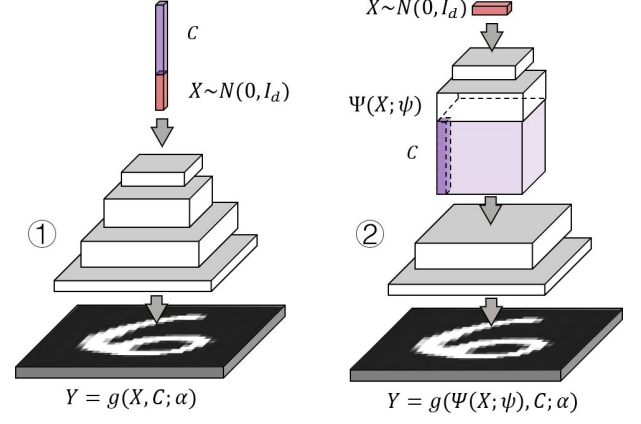


Fig. 3. Network architecture of initializer (category-to-image synthesis). (1) early concatenation: a top-down ConvNet takes as input the concatenation of the condition vector C and the latent noise vector $X \sim N(0, I_d)$, and outputs an image Y . (2) late concatenation: a top-down ConvNet takes as input only the latent noise vector $X \sim N(0, I_d)$, and outputs an image Y , in which the condition C is concatenated with the output of an intermediate layer. g parameterized by α is the sub-network after concatenation, while Ψ parameterized by ψ is the sub-network before concatenation.

of convolutions and ReLU non-linear transformation. (See Figure 4(2) for an illustration.) The configuration of the networks will be discussed in the section of each experiment.

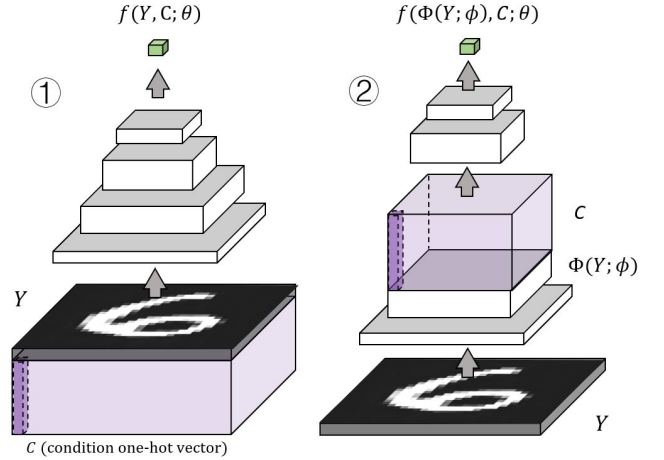


Fig. 4. Network architecture of solver (category-to-image synthesis). (1) early concatenation: a bottom-up ConvNet takes as input the depth concatenation of the spatially replicated condition C and the image Y , and outputs the negative energy. (2) late concatenation: a bottom-up ConvNet takes as input only the image Y , and outputs the negative energy, in which the condition C is concatenated with the output of an intermediate layer. f parameterized by θ is the sub-network after concatenation, while Φ parameterized by ϕ is the sub-network before concatenation.

4.1.2 Conditional image generation on MNIST dataset

We first learn our model on MNIST [33] handwritten digit images conditioned on their class labels, which are encoded as one-hot vectors.

We adopt the setting of “early concatenation” for the initializer. $g(X, C; \alpha)$ is a generator that maps the $1 \times 1 \times 110$ concatenated result (The dimension of X is 100, and the size of C is 10.) to a 28×28 grayscale image by 4 layers of deconvolutions with kernel

sizes $\{5, 5, 5, 5\}$, up-sampling factors $\{1, 2, 2, 2\}$ and numbers of output channels $\{256, 128, 64, 1\}$ at different layers. The last deconvolution is followed by tanh operation, and the others are followed by batch normalization and ReLU operations.

We adopt the setting of “late concatenation” for the solver. $\Phi(Y; \phi)$ consists of 2 layers of convolutions with filter sizes $\{5, 3\}$, down-sampling factors $\{2, 2\}$ and numbers of output channels $\{64, 128\}$. The concatenated output is of size $7 \times 7 \times 138$. (The number of the output channels of Φ is 128, and the size of C is 10.) $f(\Phi(Y; \phi), C; \theta)$ is a 2-layer ConvNet, where the first layer has $256 \ 3 \times 3$ filters, and the last layer is a fully connected layer with 100 filters.

We use the Adam [34] for optimization. The joint models are trained with mini-batches of size 200. The number of paralleled MCMC chains is also 200. Figure 5 shows some of the generated samples conditioned on the class labels after training. Each column is conditioned on one label and each row is a different generated sample.

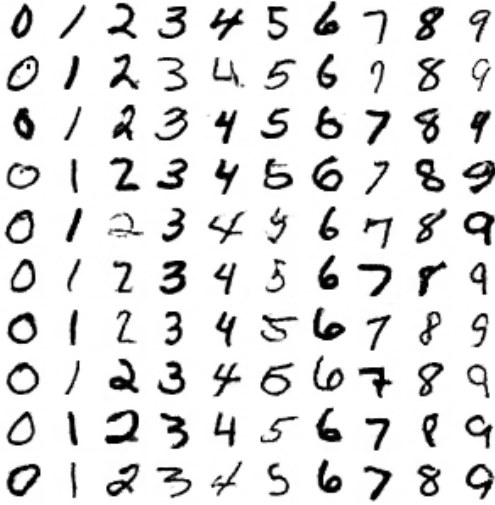


Fig. 5. Generated MNIST handwritten digits. Each column is conditioned on one class label and each row is a different synthesized sample. The size of the generated images is 64×64 .

To evaluate the learned conditional distribution, Table 1 shows Gaussian Parzen window log-likelihood estimates of the MNIST test set. We sample 10,000 examples from the learned conditional distribution by first sampling the class label C from the uniform prior distribution, and X from $N(0, I_d)$, then the initializer $g(X_i, C_i; \alpha)$ and the solver model $p(Y|\Psi(C_i; \psi); \theta)$ cooperatively generate the synthesized example from the sampled C_i and X_i . A Gaussian Parzen window is fitted to these synthesized examples, and the log-likelihood of the test set using the Parzen window distribution is estimated. The standard deviation of the Gaussians is obtained by cross validations. We follow the same procedure as [5] for computing the log-likelihood estimates for fair comparison. As shown in Table 1, both initializer and solver can achieve better results than other baseline methods.

4.1.3 Conditional image generation on Cifar-10

We also test the proposed framework on Cifar-10 [37] object dataset, which contains 10-class 60,000 training images of 32×32 pixels. Compared with the MNIST dataset, Cifar-10 contains training images with more complicated visual patterns.

TABLE 1
Parzen window-based log-likelihood estimates for MNIST.

Model	log-likelihood
DBN [35]	138 ± 2.0
Stacked CAE [35]	121 ± 1.6
Deep GSN [36]	214 ± 1.1
GAN [5]	225 ± 2.0
Conditional GAN [6]	132 ± 1.8
initializer (ours)	239 ± 2.1
solver (ours)	240 ± 2.1

TABLE 2
Inception scores on Cifar-10 dataset.

Model	Inception score
Conditional GAN [38]	6.58
Conditional SteinGAN [39]	6.35
initializer (ours)	6.63
solver (ours)	7.30

As to the initializer, we adopt the “late concatenation” setting. Specifically, $\Psi(X; \psi)$ is a decoder that maps 100-dimensional X (i.e., $1 \times 1 \times 100$) to an intermediate output with spatial dimension 8×8 by 2 layers of deconvolutions with kernel sizes $\{4, 5\}$, up-sampling factors $\{1, 2\}$ and numbers of output channels $\{256, 128\}$ at different layers from top to bottom, respectively. The condition C is a 10-dimensional one-hot vector to represent class. $g(\Psi(X; \psi), C; \alpha)$ is a generator that maps the $8 \times 8 \times 138$ concatenated result to a $32 \times 32 \times 3$ image by 2 layers of deconvolutions with kernel sizes $\{5, 5\}$, up-sampling factors $\{2, 2\}$ and numbers of output channels $\{64, 3\}$ at different layers.

We adopt the “late concatenation” setting for the solver. $\Phi(Y; \phi)$ consists of 2 layers of convolutions with filter sizes $\{5, 3\}$, down-sampling factors $\{2, 2\}$ and numbers of output channels $\{64, 128\}$. The concatenated output is of size $8 \times 8 \times 138$. $f(\Phi(Y; \phi), C; \theta)$ is a 2-layer bottom-up ConvNet, where the first layer has $256 \ 3 \times 3$ filters, and the last layer is a fully connected layer with 100 filters.

We use Adam to optimize the solver with initial learning rate 0.002, $\beta_1 = 0.5$ and $\beta_2 = 0.999$, and the initializer with initial learning rate 0.0064, $\beta_1 = 0.5$ and $\beta_2 = 0.999$. The mini-batch size is 300. The number of paralleled MCMC chains is 300. The number of Langevin dynamics steps is 8. The step size δ of Langevin dynamics is 0.0008. The standard deviation of the residual in the initializer is $\sigma = 0.3$, and the standard deviation of the reference distribution in the solver is 0.016. We run 2,000 epochs to train the model, where we disable the noise term in Langevin dynamics in the last 1,500 ones.

Figure 6 shows the generated object patterns. Each row is conditioned on one category. The first two columns display some typical training examples, while the rest columns show generated images conditional on labels. We evaluate the learned conditional distribution by computing the inception scores of the generated examples. Table 2 compares our framework against two baselines, which are two conditional models based on GANs. The proposed model performance better than the baselines. We also found that in the proposed method, the solution provided by the initializer is indeed further refined by the solver in terms of inception score.

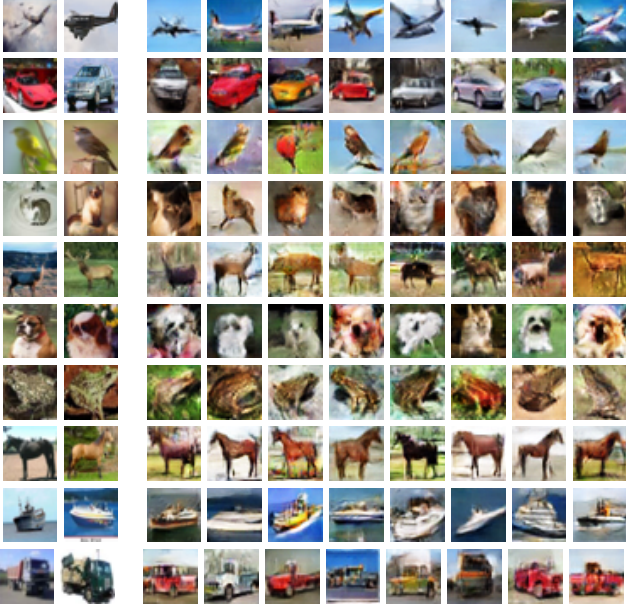


Fig. 6. Generated Cifar-10 object images. Each row is conditioned on one category label. The first two columns are training images, and the remaining columns display generated images conditioned on their labels. The image size is 32×32 pixels. The categories are airplane, automobile, bird, cat, deer, dog, frog, horse, ship, and truck from top to bottom.

4.1.4 Disentangling style and category

We test the inference power of the initializer, trained jointly with the solver, by applying it to a task of style transfer from an unseen testing image onto other categories. The models are trained on SVHN [40] dataset that contains 10 classes of digits collected from street view house numbers. The network architectures of initializer and solver are similar to those used in Section 4.1.2, except that the training images in this experiment are RGB images and they are of size 32×32 pixels. With the learned initializer, we first infer the latent variables X corresponding to that testing image. We then fix the inferred latent vector, change the category label C , and generate the different categories of images with the same style as the testing image by the learned model. Given a testing image Y with known category label C , the inference of the latent vector X can be performed by directly sampling from the posterior distribution $p(X|Y, C; \alpha)$ via Langevin dynamics, which iterates

$$X_{\tau+1} = X_{\tau} + sU_{\tau} + \frac{s^2}{2} \left[\frac{1}{\sigma^2} (Y - g(X_{\tau}, C; \alpha)) \frac{\partial}{\partial X} g(X_{\tau}, C; \alpha) - X_{\tau} \right]. \quad (19)$$

If the category label of the testing image is unknown, we need to infer both C and X from Y . Since C is a one-hot vector, in order to adopt a gradient-based method to infer C , we adopt a continuous approximation by reparametrizing C using a softMax transformation on the auxiliary continuous variables A . Specifically, let $C = (c_k, k = 1, \dots, K)$ and $A = (a_k, k = 1, \dots, K)$, we reparametrize $C = v(A)$ where $c_k = \exp(a_k) / \sum_k \exp(a'_k)$, for $k = 1, \dots, K$, and assume the prior for A to be $N(0, I_K)$. Then the Langevin dynamics for sampling $A \sim p(A|Y, X)$ iterates

$$A_{\tau+1} = A_{\tau} + sU_{\tau} + \frac{s^2}{2} \left[\frac{1}{\sigma^2} (Y - g(X_{\tau}, v(A); \alpha)) \frac{\partial}{\partial A} g(X_{\tau}, v(A); \alpha) - A \right]. \quad (20)$$

Figure 7 shows 10 results of style transfer. For each testing image Y , we infer X and C by sampling $[X, C] \sim p(X, C|Y)$, which iterates (1) $X \sim p(X|Y, C)$, and (2) $C = v(A)$ where $A \sim p(A|Y, X)$, with randomly initialized X and C . We then fix the inferred latent vector X , change the category label C , and generate images from the combination of C and X by the learned models. This demonstrates the disentanglement of style from category.



Fig. 7. Style transfer. The trained initializer can disentangle the style and the category such that the style information can be inferred from a testing image and transferred to other categories. The first column shows testing images. The other columns show style transfer by the model, where the style latent variable X of each row is set to the value inferred from the testing image in the first column by the Langevin inference. Each column corresponds to a different category label C . The image size is 32×32 pixels.

4.2 Experiment 2: Image \rightarrow Image

4.2.1 Network architecture

We study learning conditional distribution for image-to-image translation by our framework. The network architecture of the model in this experiment is given as follows.

As to the initializer, a straightforward design is given as follows: we first sample X from the Gaussian noise prior $N(0, I_d)$, and we encode the conditional image C via an encoder $\Phi(C; \phi)$ parametrized by ϕ . The image embedding $\Phi(C_i)$ is then concatenated to the latent noise vector X_i . After this, we generate target image Y_i by a generator $g(X, \Phi(C_i; \phi); \alpha)$. With Gaussian noise X , the initializer will produce stochastic outputs as a distribution. See Figure 8(1) for an illustration of the structure. However, in initial experiments, we found that this design was ineffective in the sense that the generator learned to ignore the noise and produce deterministic outputs. Inspired by [11], we design the initializer by following a general shape of a “U-Net” [41] with the form of dropout [42], applied on several layers, as noise that accounts for stochasticity in this experiment. A “U-Net” is an encoder-decoder structure with skip connections added between each layer j and layer $M - j$. (M is the number of layers.) Each skip connection performs a concatenation between all channels at layer j and those at layer $M - j$. In the task of image-to-image translation, the input

and output images usually differ in appearance but share low-level information. For example, in the case of translating sketch image to photo image, the input and output images are roughly aligned in outline except that they have different colors and textures in appearance. The addition of skip connections allow direct transfer of low-level information across the network. Figure 8(2) illustrates the U-Net structure with dropout as the initializer for image-to-image translation.

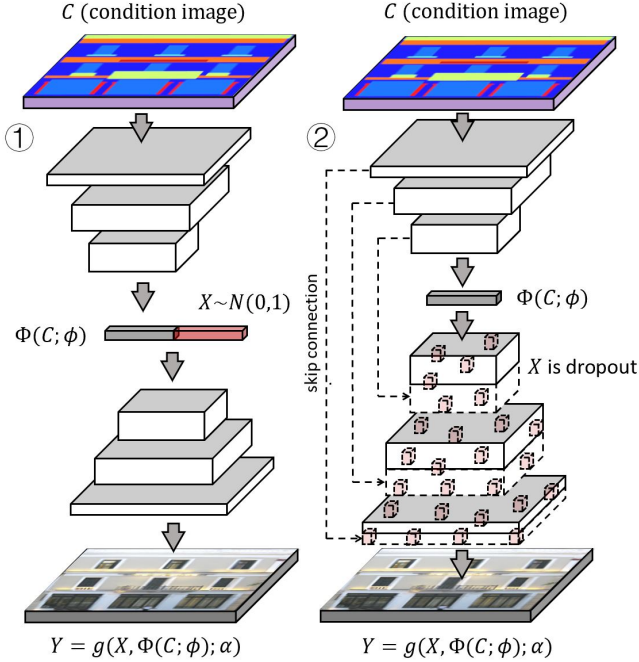


Fig. 8. Network architecture of initializer (image-to-image translation). (1) naive straightforward design: the condition image C is first encoded to a vector representation by an encoder $\Phi(C; \phi)$ parameterized by ϕ , and then the vector is concatenated with the Gaussian noise vector X . A generator g parameterized by α takes as input the concatenated vector and outputs an image Y . (2) U-Net with dropout: an encoder-decoder structure (Φ is the encoder parameterized by ϕ and g is the decoder parameterized by α), with skip connections added between each layer j and layer $M - j$, where M is the number of layers. Each skip connection concatenates all channels at layer j and those at layer $M - j$. The dropout is applied to each layer in the decoder g to account for randomness X .

As to the design of the solver model, we first perform channel concatenation on target image Y and conditional image C , where both images are of the same size. The negative energy function is then defined by a bottom-up ConvNet $f(Y, C; \theta)$, which maps the 6-channel “image” to a negative energy by several convolutional layers. Leaky ReLU layers are used between convolutional layers. Figure 9 shows an illustration of the solver structure.

4.2.2 Semantic labels \rightarrow Scene images

The experiments are conducted on CMP Facade dataset [43] where each building facade image is associated with an image of architectural labels. The condition image and the target image are of the size of 256×256 pixels with RGB channels. Data are randomly split into training and testing sets.

In the initializer, the encoder Φ consists of 8 layers of convolutions with a filter size 4, a subsampling factor 2, and the numbers of channels $\{64, 128, 256, 512, 512, 512, 512, 512\}$ at different layers. Batch normalization and leaky ReLU (with slope 0.2) layers are used after each convolutional layer except that batch normalization is not applied after the first layer. The

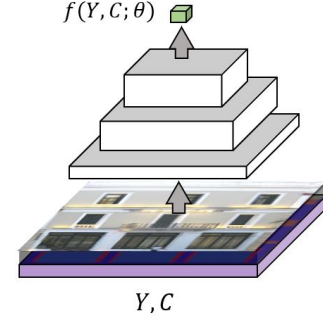


Fig. 9. Network architecture of solver (image-to-image translation). Channel concatenation is performed on the condition image C and the target image Y . The resulting 6-channel “image” is then fed into a bottom-up ConvNet $f(Y, C; \theta)$. The output of f serves as a negative energy in the solver model.

output of Φ is then fed into g , which consists of 8 layers of deconvolutions with a kernel size 4, an up-sampling factor 2, and the numbers of channels $\{512, 512, 512, 512, 256, 128, 64, 3\}$ at different layers. Batch normalization, dropout with a dropout rate of 0.5, and ReLU layers are used between deconvolutional layers and tanh non-linearity is used after the last layer. The U-Net structure used in this experiment is a connection of the encoder Φ and the decoder g , along with skip connections added to concatenate activations of each layer j and layer $M - j$. (M is the total number of layers.) Therefore, the numbers of output channels of g in the U-Net are $\{1024, 1024, 1024, 1024, 512, 256, 128, 3\}$. The dropout that is applied to each layer of g implies an implicit latent factor X in the initializer. In the training stage, there is no need to infer this X . The cooperative training scheme can get around the difficulty of the inference of any complicated form of latent factors by MCMC teaching, i.e., in each iteration, the learning of the initializer $g(X, \Phi(C; \phi); \alpha)$ is based on how the MCMC changes the initial examples generated by the initializer with condition C and dropout X .

In the solver model, we first perform channel concatenation on target image Y and conditional image C , where both images are of size $256 \times 256 \times 3$. The negative energy function is then defined by a 4-layer bottom-up ConvNet $f(Y, C; \theta)$, which maps the 6-channel “image” to negative energies by 3 convolutional layers with numbers of channels $\{64, 128, 256\}$, filter sizes $\{5, 3, 3\}$ and subsampling factors $\{2, 2, 1\}$ at different layers (from bottom to top), and one fully connected layer with 100 single filters. Leaky ReLU layers are used between convolutional layers.

Adam is used to optimize the solver with initial learning rate 0.007, and the initializer with initial learning rate 0.0001. We set mini-batch size to be 1. The number of paralleled MCMC chains is also 1. We run 15 Langevin steps with a step size $\delta = 0.002$. The standard deviation of the residual in the initializer is $\sigma = 0.3$. The standard deviation of the reference distribution in the solver is 0.016. We run 3,000 epochs to train our model.

We adopt random jitter and mirroring for data augmentation in the training stage. As to random jitter, we first resize the 256×256 input images to 286×286 ones, and then randomly crop image patches with a size 256×256 .

We found it beneficial to feed both the refined solutions and the observed ground truth solutions to the initializer in this task. The solver’s job remains unchanged, but the initializer is tasked to not only learn from the solver but also to be near the ground truth

solution. We adopts ℓ_1 distance to measure how close the initializer and the observed solutions are. [11] also find this strategy effective.

As to the computational time, our method includes four key steps in each iteration, as shown in Algorithm 1. Comparing with GAN-based method, our framework has additional l steps of Langevin. We set $l = 15$. However, the Langevin is based on gradient, whose computation can be powered by back-propagation, so it is not time-consuming. To be concrete, our method costs 32.7s, while GAN-based method costs 30.9s per epoch in a PC with an Intel i7-6700k CPU and a Titan Xp GPU in this experiment.

Figure 10 shows some qualitative results of generating building facade images from the semantic labels. The first row displays 6 semantic label images that are unseen in the training data. The second row displays the corresponding ground truth images for reference. The results by a baseline method [11] are shown in the third row for comparison. [11] is a conditional GAN method for image-to-image mapping. Since its generator also uses a “U-Net” and is paired up with a ℓ_1 loss, for a fair comparison, our initializer adopts exactly the same “U-Net” structure as in [11]. The fourth and fifth rows show the generated results conditioned on the images shown in the first row by the learned initializer and solver respectively.

We perform a human perceptual test for evaluating the visual quality of synthesized images. We randomly select 50 different human users to participate in this test. Each participant is first presented two images at a time, which are results generated by two different methods given the same conditional input, and then asked which one looks more like a real image. We have total 100 pairwise comparisons for each participant. We evaluate each algorithm by the ratio that the results generated by the algorithm are preferred. As shown in Table 3, the results generated by our method are considered more realistic by the human subjects. We also test the ℓ_1 effect in Table 3 as an ablation study and conform its effectiveness of improving the visual quality of the generated image patterns.

TABLE 3
Human perceptual test for image-to-image synthesis.

methods	human preference ratio
solver with ℓ_1 / pixel2pixel	0.63 / 0.37
solver with ℓ_1 / solver without ℓ_1	1.00 / 0.00

4.2.3 Sketch images \rightarrow Photo images

We next test the model on CUHK Face Sketch database (CUFS) [44], where for each face, there is a sketch drawn by an artist based on a photo of the face. We learn to recover the color face images from the sketch images by the proposed framework. The network design and hyperparameter setting are similar to the one we used in Section 4.2.2, except that the mini-batch size and the number of paralleled MCMC chains are set to be 4.

Figure 11(a) displays the face image synthesis results conditioned on the sketch images. The first and second rows show some sketch images, while the third and fourth rows show the corresponding recovered images obtained by sampling from the learned conditional distribution. From the results, we can see that the generated facial appearance (color and texture) in each output image is not only reasonable but also consistent with the input sketch face image in the sense that the face identity in each input sketch image remains unchanged after being translating to a photo image.

Figure 11(b) demonstrates the learned sketch (condition) manifold by showing 4 examples of interpolation. For each row, the sketch images at the two ends are first encoded into the embedding by $\Phi(C)$, and then each face image in the middle is obtained by first interpolating the sketch embedding, and then generating the images using the initializer with a fixed dropout, and eventually refining the results by the solver via Langevin dynamics. Even though there is no ground-truth sketch images for the intervening points, the generated faces appear plausible. Since the dropout X is fixed, the only changing factor is the sketch embedding. We observe smooth changing of the outline of the generated faces.

We conduct another experiment on UT Zappos50K dataset [43] for photo image recovery from edge image. The dataset contains 50k training images of shoes. Edge images are computed by HED edge detector [45] with post processing. We use the same model structure as the one in the last experiment. Figure 12 shows some qualitative results of synthesizing shoe images from edge images.

4.2.4 Image inpainting

We also test our method on the task of image inpainting by learning a mapping from an occluded image (256×256 pixels), where a mask with the size of 128×128 pixels is centrally placed onto the original version, to the original image. We use Paris streetview [46] and the CMP Facade dataset. In this case, C is the observed part of the input image, and Y is the unobserved part of the image. The network architectures for both initializer and solver, along with hyperparameter setting, are similar to those we used in Section 4.2.2. To recover the occluded part of the input images, we only update the pixels of the occluded region of each image in the Langevin dynamics.

Figure 13 shows a qualitative comparison of our method and the conditional GAN [11] on the CMP Facade dataset. Each column displays one example. The first image is the testing image with a hole that needs to be recovered, the second image shows the ground truth, the third image shows the result recovered by the conditional GAN as a comparison. The fourth image shows the result recovered by the initializer, and the last image shows the result recovered by the solver.

Table 4 shows quantitative results where the recovery performance is measured by the peak signal-tonoise ratio (PSNR) and structural similarity measures (SSIM), which are computed between the occlusion regions of the generated example and the ground truth example. The batch size is one. Our method outperforms the baseline in this recovery task.

TABLE 4
Comparison with the baseline method for image inpainting on CMP Facade dataset and Paris streetview dataset.

	CMP Facades		Paris streetview	
	PSNR	SSIM	PSNR	SSIM
conditional GAN	19.3411	0.739	15.17	0.745
ours	20.4678	0.767	21.17	0.785

5 CONCLUSION

Solving a challenging problem usually requires an iterative algorithm. This amounts to slow thinking. The iterative algorithm usually requires a good initialization to jumpstart it so that it can converge quickly. The initialization amounts to fast thinking. For instance, reasoning and planning usually require iterative search



Fig. 10. Generating images conditioned on architectural labels. The first row displays 6 condition images with architectural labels. The second row displays the corresponding ground truth images for reference. For comparison, the third row shows the generated results by a baseline method, which is the conditional GAN. The fourth and fifth rows present the generated results obtained by the learned initializer and solver respectively. The training images are of the size 256×256 pixels.

or optimization, which can be initialized by a learned computation in the form of a neural network. Thus integrating fast thinking initialization and slow thinking sampling or optimization is very compelling.

This paper addresses the problem of high-dimensional conditional learning and proposes a cooperative learning method that couples a fast thinking initializer and a slow thinking solver. The initializer initializes the iterative optimization or sampling process of the solver, while the solver in return teaches the initializer by distilling its iterative algorithm into the initializer. We demonstrate the proposed method on a variety of image synthesis and recovery tasks.

Compared to GAN-based method, such as conditional GANs, our method is equipped with an extra iterative sampling and optimization algorithm to refine the solution, guided by a learned objective function. This may prove to be a powerful method for solving challenging conditional learning problems. Integrating fast thinking and slow thinking may also be of interest to cognitive

science. We will consider applying such a framework to cognitive science and imitation learning in our future work.

ACKNOWLEDGMENTS

We gratefully acknowledge the support of NVIDIA Corporation with the donation of the Titan Xp GPU used for this research. The work is supported by Hikvision gift fund, DARPA SIMPLEX N66001-15-C-4035, ONR MURI N00014-16-1-2007, DARPA ARO W911NF-16-1-0579, and DARPA N66001-17-2-4029. We thank Erik Nijkamp for his help on coding. We thank Siyuan Huang for helpful discussions.

REFERENCES

- [1] P. Abbeel and A. Y. Ng, “Apprenticeship learning via inverse reinforcement learning,” in *Proceedings of the Twenty-first International Conference on Machine Learning (ICML)*, 2004, pp. 1–8.

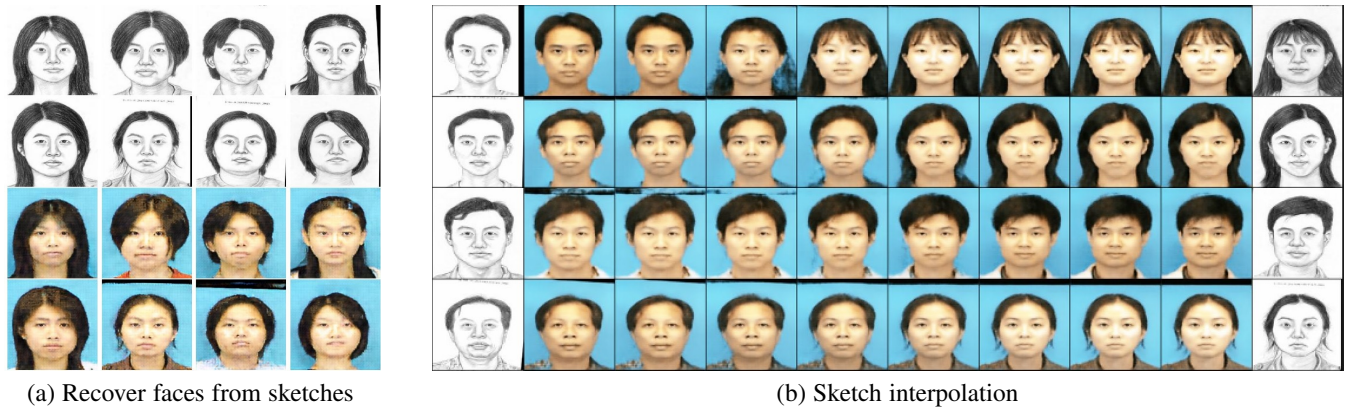


Fig. 11. (a) Sketch-to-photo face synthesis. The first and second rows: sketch images as conditions. The third and fourth rows: corresponding face images sampled from the learned models conditioned on sketch images. (b) Sketch interpolation: Generated face images by interpolating between the embedding of the sketch images at two ends, with fixed dropout. Each row displays one example of interpolation.



Fig. 12. Example results on edges \rightarrow shoes generation, compared to ground truth. The first row displays the edge images. The second row shows the corresponding ground truth photo images. The last two rows present the generated results obtained by the initializer and the solver, respectively.

- [2] B. D. Ziebart, A. L. Maas, J. A. Bagnell, and A. K. Dey, "Maximum entropy inverse reinforcement learning," in *Twenty-Third AAAI Conference on Artificial Intelligence*, 2008, pp. 1433–1438.
- [3] J. Ho and S. Ermon, "Generative adversarial imitation learning," in *Advances in Neural Information Processing Systems*, 2016, pp. 4565–4573.
- [4] J. J. Hopfield, "Neural networks and physical systems with emergent collective computational abilities," *Proceedings of the National Academy of Sciences*, vol. 79, no. 8, pp. 2554–2558, 1982.
- [5] I. Goodfellow, J. Pouget-Abadie, M. Mirza, B. Xu, D. Warde-Farley, S. Ozair, A. Courville, and Y. Bengio, "Generative adversarial nets," in *Advances in Neural Information Processing Systems*, 2014, pp. 2672–2680.
- [6] M. Mirza and S. Osindero, "Conditional generative adversarial nets," *arXiv preprint arXiv:1411.1784*, 2014.
- [7] E. L. Denton, S. Chintala, R. Fergus *et al.*, "Deep generative image models using a laplacian pyramid of adversarial networks," in *Advances in Neural Information Processing Systems*, 2015, pp. 1486–1494.
- [8] S. Reed, Z. Akata, X. Yan, L. Logeswaran, B. Schiele, and H. Lee, "Generative adversarial text to image synthesis," *arXiv preprint arXiv:1605.05396*, 2016.
- [9] H. Zhang, T. Xu, H. Li, S. Zhang, X. Huang, X. Wang, and D. Metaxas, "Stackgan: Text to photo-realistic image synthesis with stacked generative adversarial networks," in *IEEE Int. Conf. Comput. Vision (ICCV)*, 2017, pp. 5907–5915.
- [10] X. Wang and A. Gupta, "Generative image modeling using style and structure adversarial networks," in *European Conference on Computer Vision*. Springer, 2016, pp. 318–335.
- [11] P. Isola, J.-Y. Zhu, T. Zhou, and A. A. Efros, "Image-to-image translation with conditional adversarial networks."
- [12] J.-Y. Zhu, T. Park, P. Isola, and A. A. Efros, "Unpaired image-to-image translation using cycle-consistent adversarial networks," in *Proceedings of the IEEE international conference on computer vision*, 2017, pp. 2223–2232.
- [13] M.-Y. Liu, T. Breuel, and J. Kautz, "Unsupervised image-to-image translation networks," in *Advances in Neural Information Processing Systems*, 2017, pp. 700–708.
- [14] C. Ledig, L. Theis, F. Huszar, J. Caballero, A. Cunningham, A. Acosta, A. Aitken, A. Tejani, J. Totz, Z. Wang *et al.*, "Photo-realistic single image super-resolution using a generative adversarial network," in *Proceedings of the IEEE Conference on Computer Vision and Pattern Recognition*, 2017, pp. 4681–4690.
- [15] J. Xie, Y. Lu, R. Gao, and Y. N. Wu, "Cooperative learning of energy-based model and latent variable model via mcmc teaching," in *AAAI*, 2018.
- [16] J. Lafferty, A. McCallum, and F. C. Pereira, "Conditional random fields: Probabilistic models for segmenting and labeling sequence data," 2001.
- [17] E. P. Xing, R. Yan, and A. G. Hauptmann, "Mining associated text and images with dual-wing harmoniums," *arXiv preprint arXiv:1207.1423*, 2012.
- [18] J. Ngiam, A. Khosla, M. Kim, J. Nam, H. Lee, and A. Y. Ng, "Multimodal deep learning," in *Proceedings of the 28th international conference on machine learning (ICML-11)*, 2011, pp. 689–696.
- [19] N. Srivastava and R. R. Salakhutdinov, "Multimodal learning with deep boltzmann machines," in *Advances in neural information processing systems*, 2012, pp. 2222–2230.
- [20] J. Xie, Y. Lu, S.-C. Zhu, and Y. N. Wu, "A theory of generative convnet," in *International Conference on Machine Learning*, 2016.
- [21] R. Gao, Y. Lu, J. Zhou, S.-C. Zhu, and Y. Nian Wu, "Learning generative ConvNets via multi-grid modeling and sampling," in *Proceedings of the IEEE Conference on Computer Vision and Pattern Recognition*, 2018, pp. 9155–9164.
- [22] J. Xie, S.-C. Zhu, and Y. N. Wu, "Synthesizing dynamic patterns by spatial-temporal generative convnet," in *CVPR*, 2017.
- [23] J. Xie, S.-C. Zhu, and Y.-N. Wu, "Learning energy-based spatial-temporal generative ConvNets for dynamic patterns," *IEEE transactions on pattern analysis and machine intelligence*, 2019.
- [24] J. Xie, Z. Zheng, R. Gao, W. Wang, S.-C. Zhu, and Y. N. Wu, "Learning descriptor networks for 3D shape synthesis and analysis," in *Proceedings of the IEEE Conference on Computer Vision and Pattern Recognition*, 2018, pp. 8629–8638.
- [25] E. Nijkamp, M. Hill, S.-C. Zhu, and Y. N. Wu, "Learning non-convergent non-persistent short-run mcmc toward energy-based model," in *Advances in Neural Information Processing Systems*, 2019, pp. 5233–5243.
- [26] E. Nijkamp, M. Hill, T. Han, S.-C. Zhu, and Y. N. Wu, "On the anatomy of mcmc-based maximum likelihood learning of energy-based models," *arXiv preprint arXiv:1903.12370*, 2019.
- [27] A. Krizhevsky, I. Sutskever, and G. E. Hinton, "Imagenet classification with deep convolutional neural networks," in *NIPS*, 2012, pp. 1097–1105.



Fig. 13. Example results of photo inpainting. Each column displays one example. The first image is the testing image (256×256 pixels) with a hole of 128×128 pixels that needs to be recovered, the second image displays the ground truth as a reference, the third image shows the result recovered by the conditional GAN as a comparison. The fourth and fifth images show the results recovered by the initializer and the solver, respectively.

- [28] L. Younes, “On the convergence of markovian stochastic algorithms with rapidly decreasing ergodicity rates,” *Stochastics: An International Journal of Probability and Stochastic Processes*, vol. 65, no. 3-4, pp. 177–228, 1999.
- [29] T. Han, Y. Lu, S.-C. Zhu, and Y. N. Wu, “Alternating back-propagation for generator network,” 2017.
- [30] G. E. Hinton, “Training products of experts by minimizing contrastive divergence,” *Neural Computation*, vol. 14, no. 8, pp. 1771–1800, 2002.
- [31] J. Xie, Y. Lu, R. Gao, S.-C. Zhu, and Y. N. Wu, “Cooperative training of descriptor and generator networks,” *arXiv preprint arXiv:1609.09408*, 2016.
- [32] S. Ioffe and C. Szegedy, “Batch normalization: Accelerating deep network training by reducing internal covariate shift,” *arXiv preprint arXiv:1502.03167*, 2015.
- [33] Y. LeCun, L. Bottou, Y. Bengio, P. Haffner *et al.*, “Gradient-based learning applied to document recognition,” *Proceedings of the IEEE*, vol. 86, no. 11, pp. 2278–2324, 1998.
- [34] D. P. Kingma and J. Ba, “Adam: A method for stochastic optimization,” *arXiv preprint arXiv:1412.6980*, 2014.
- [35] Y. Bengio, G. Mesnil, Y. Dauphin, and S. Rifai, “Better mixing via deep representations,” in *International Conference on Machine Learning*, 2013, pp. 552–560.
- [36] Y. Bengio, E. Laufer, G. Alain, and J. Yosinski, “Deep generative stochastic networks trainable by backprop,” in *International Conference on Machine Learning*, 2014, pp. 226–234.
- [37] A. Krizhevsky, “Learning multiple layers of features from tiny images,” Citeseer, Tech. Rep., 2009.
- [38] T. Salimans, I. Goodfellow, W. Zaremba, V. Cheung, A. Radford, and X. Chen, “Improved techniques for training gans,” in *Advances in Neural Information Processing Systems*, 2016, pp. 2234–2242.
- [39] D. Wang and Q. Liu, “Learning to draw samples: With application to amortized mle for generative adversarial learning,” *arXiv preprint arXiv:1611.01722*, 2016.
- [40] Y. Netzer, T. Wang, A. Coates, A. Bissacco, B. Wu, and A. Y. Ng, “Reading digits in natural images with unsupervised feature learning,” in *NIPS workshop on deep learning and unsupervised feature learning*, vol. 2011, no. 2, 2011, p. 5.
- [41] O. Ronneberger, P. Fischer, and T. Brox, “U-net: Convolutional networks for biomedical image segmentation,” in *International Conference on Medical image computing and computer-assisted intervention*. Springer, 2015, pp. 234–241.
- [42] N. Srivastava, G. Hinton, A. Krizhevsky, I. Sutskever, and R. Salakhutdinov, “Dropout: a simple way to prevent neural networks from overfitting,” *The journal of machine learning research*, vol. 15, no. 1, pp. 1929–1958, 2014.
- [43] R. Tyleček and R. Šára, “Spatial pattern templates for recognition

- of objects with regular structure,” in *German Conference on Pattern Recognition*. Springer, 2013, pp. 364–374.
- [44] X. Wang and X. Tang, “Face photo-sketch synthesis and recognition,” *IEEE Transactions on Pattern Analysis and Machine Intelligence*, vol. 31, no. 11, pp. 1955–1967, 2009.
 - [45] S. Xie and Z. Tu, “Holistically-nested edge detection,” in *Proceedings of the IEEE international conference on computer vision*, 2015, pp. 1395–1403.
 - [46] D. Pathak, P. Krahenbuhl, J. Donahue, T. Darrell, and A. A. Efros, “Context encoders: Feature learning by inpainting,” in *Proceedings of the IEEE conference on computer vision and pattern recognition*, 2016, pp. 2536–2544.